

## Lecture Notes

Lecture: Accelerator Physics  
Winter 2024/25

# Synchrotron and Undulator Radiation

Axel Bernhard

## Contents

<b>1</b>	<b>Introduction</b>	<b>3</b>
<b>2</b>	<b>Moving point charges</b>	<b>12</b>
2.1	System of units . . . . .	12
2.2	Integration of the inh. Maxwell equations . . . . .	13
2.3	Solution for the point charge . . . . .	15
2.4	Derivation of the fields . . . . .	17
2.5	Emitted power . . . . .	19
2.6	Transverse and longitudinal acceleration . . . . .	20

# 1 Introduction: What are and why are synchrotron radiation sources?

## Accelerated charges emit electromagnetic waves



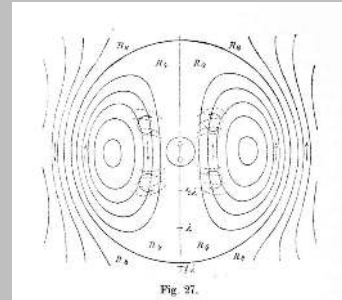
(Krewaldt 1894)

Heinrich Hertz  
(1857-1894)



(Stodart 1890)

James Clerk  
Maxwell  
(1831-1879)



H. HERTZ: UNTERSUCHUNGEN UEBER DIE AUSBREITUNG DER ELEKTRISCHEN KRAFT (1892)

Fig.: Calculation of the radiation characteristic of a transmitting antenna by applying Maxwell's equations. 1888 Hertz succeeded in experimentally proving the existence of electromagnetic waves and thereby the confirmation of the Maxwell electromagnetic theory of light.

The frequency range of the classical Hertz dipole lies within the MHz range. Visible light or even X-rays are emitted only in the relativistic case.

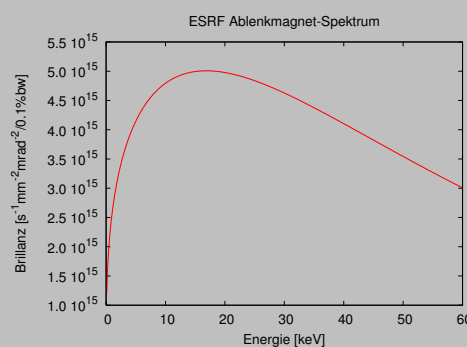
## The relativistic Doppler effect extends the spectrum into the X-ray range

- *Dilatation* of the moving particles *proper time*
- *Boost* of the radiation frequency in the laboratory frame by  $\gamma^3$



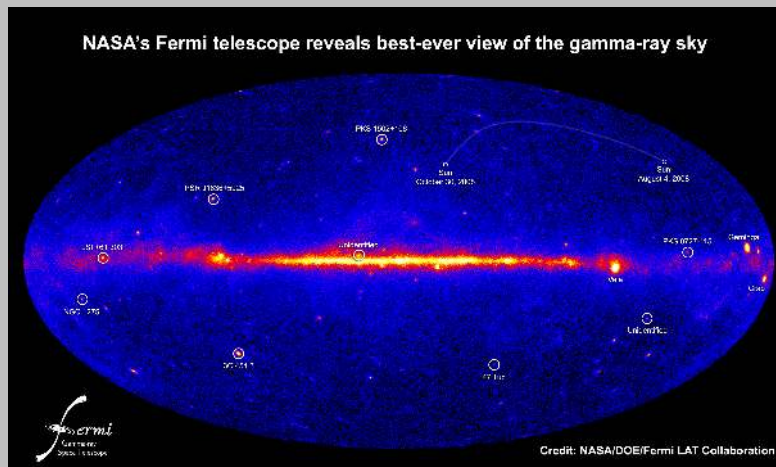
Albert Einstein  
(1879-1955)

(Schmutzer 1921)



Even if the term *synchrotron radiation* seems exotic, it is a fundamental physical phenomenon that also occurs in nature.

### Natural synchrotron radiation



(NASA - Fermi's Best-Ever Look at the Gamma-Ray Sky 2020)

The galactic centre is emitting X-rays

### Cosmic synchrotron radiation sources

#### X-ray sources

are for example supernova remnants



NASA, ESA, Hubble Heritage Team



NASA/CXC/SAO

Crab nebula (left: Hubble Space Telescope, top: detail, X-ray telescope Chandra)

The (microscopic) physical cause of the cosmic X-ray radiation is the deflection of relativistic electrons in the magnetic fields of other moving charges, as they occur in supernovae, cataclysmic variables, but also in single and double stars with coronal activity (see e.g. Sazanov and Revnivtsev 2006).

### Synchrotron light sources on earth

Synchrotron light sources are *particle accelerators*,



(Fenner 2013)

(Soleil 2005) designed for the *generation and use of synchrotron light*.

In “terrestrial” synchrotron radiation sources, electrons are accelerated to relativistic energies. When the particles are deflected in the dipole magnets, which keep the particles in a circular path, synchrotron radiation is released. Higher intensities can be achieved through multiple deflection in so-called insertion devices.

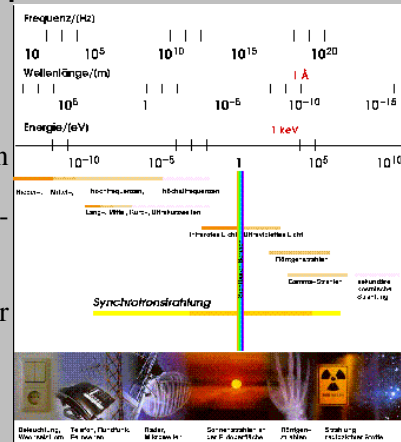
There are now four generations of synchrotron radiation sources:

1. particle accelerators for High-energy physics with parasitic use of synchrotron radiation
2. photon flux-optimised storage ring sources with use of wigglers (e.g. DORIS Hamburg, SRS Daresbury)
3. photon brilliance-optimised storage ring sources with the use of undulators (e.g. ESRF Grenoble, diamond Oxford, Soleil Paris, ALBA Barcelona, ...)
4. linear accelerator-driven sources with extremely high photon photon brilliance/coherence (e.g.: free-electron laser LCLS Stanford, FLASH, XFEL Hamburg; Energy Recovery Linac projects BERLinPro Berlin, Cornell ERL, MARS Novosibirsk)

Our local KIT synchrotron radiation source is in this count about at 2.5.

## The broad spectrum of synchrotron radiation and its applications

- spectrum from the far infrared to the hard X-ray range
- Experimental use especially of the IR and X-ray radiation
- Variety of imaging, spectroscopic and diffraction methods
- Application in Solid state physics, chemistry, molecular biology, geology, materials science, medicine...



The use of synchrotron radiation for research into (electromagnetically interacting) condensed matter is the topic of other lectures and can only be briefly touched upon here. The variety of the of analytical methods using the spectral range of X-rays is overwhelming at first sight. However, one can distinguish three main classes of methods, which are used in a multitude of combinations and modifications:

### Methods I: Imaging (spacial resolution)



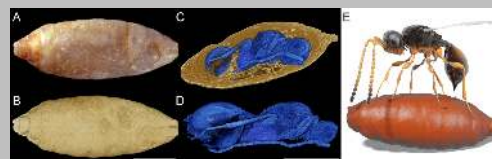
Wilhelm Conrad  
Röntgen  
(1845-1923)

(anonym 1900)

**Figure 1:** X-ray image of Albert von Kölliker's hand



(Röntgen 1896)



(van de Kamp et al. 2018)

**Figure 2:** Example for modern imaging: X-ray microtomography on petrified insect pupae with parasite (ichneumon wasp)



**Figure 3:** Example for phase contrast imaging of soft tissue: rat heart

Swiss Light Source

Albert von Kölliker was the founder of the Physikalisch-Medizinische Gesellschaft (Physical-Medical Society), where Röntgen on 23 January 1896 demonstrated the recently discovered X-rays.

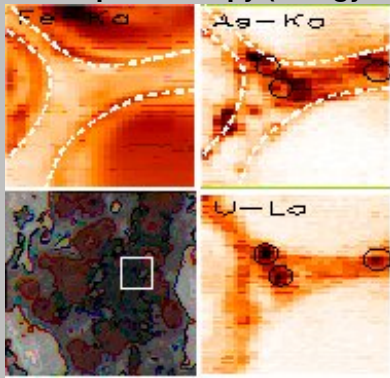
At the synchrotron, high-resolution tomograms (i.e. 3D reconstructions from 2D tomograms) can be measured with high throughput or at high speed, enabling real-time 3D X-ray movies. In the cited example, a large number of samples (fossilised insect pupae) were tomographed and

used for a systematic study of the interplay of the evolution of hosts and parasites.

The image show A: Petrified pupa of the host animal, B: Volume rendering, C: Perspective view of a parasitic wasp *Xenomorphia resurrecta*, D: female wasp *Xenomorphia resurrecta* with unfolded wings, E: Illustration of oviposition by a female ichneumon wasp into the host pupa. (van de Kamp et al. 2018).

Imaging techniques can be further differentiated according to the contrasting effect: absorption, anomalous absorption (in the vicinity of absorption edges), phase modulation (refraction), fluorescence, etc. The use of phase contrast allows X-ray imaging even on soft tissue with low absorption contrast, as shown here in the example of an absorption and a phase contrast image of a rat heart.

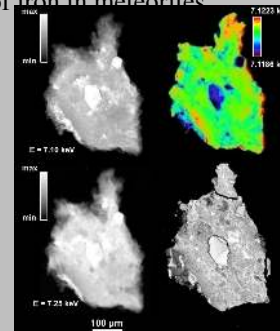
### Methods II: Spectroscopy (energy resolution)



(Denecke et al. 2005)

**Figure 4:** Example: microfluorescence mapping of trace elements in uranium-rich sediments

**Figure 5:** Example: X-Ray Absorption Near Edge Spectroscopy (XANES): Crystal chemistry of iron in meteorites



(Beck et al. 2012)

The classical spectroscopic techniques are absorption and fluorescence spectroscopy. These methods allow (via detection of the absorption edges or fluorescence lines). an identification of the elements contained in a sample and (via the fine structure of these edges or lines) of their chemical environment. The shown examples are already a combination of imaging and spectroscopic methods. In contrast to the aforementioned absorption contrast methods, where the spatial resolution is determined by the spatial resolution of the detector, the spacial resolution here is achieved by scanning the sample with a finely focussed X-ray beam. The sub-micrometre focusability is owed to one of the most prominent properties of synchrotron radiation, namely its high brilliance.

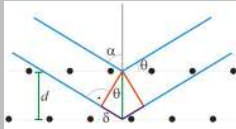
*Example.* (Fig. 4) Study of the immobilisation of radioactive elements during geogenesis. Uranium-rich “hot spots” accumulate preferentially on Fe(II) minerals. The example image shows  $120 \times 120 \mu\text{m}^2$ -element maps of the environment of an Fe(II) node. The node is surrounded by a thin layer of As, to which the uranium is bound.

Interpretation: U(VI) dissolved in groundwater is reduced in the vicinity of arsenopyrite to U(IV), which is less soluble and precipitates.

*Example.* (Fig. 5) View into the history of the solar system: transmission images of a sliver of the meteorite *Murchison* above and below the iron *K* edge (left), energy mapping of the absorption

edge (top right) and scanning electron microscope image (bottom right). The examined meteorites are carbonaceous chondrite specimens, which are considered to be fragments from the early history of our solar system. The spectroscopic data provide information on the oxidation state of the iron in these samples. This in turn allows conclusions on early reactions involving liquid water, which must have taken place on the planets or asteroids from which these fragments originated.

### Methods III: Diffraction (momentum resolution)



source: Matthias M. 2008

$$\delta = 2d \sin \theta = n\lambda$$

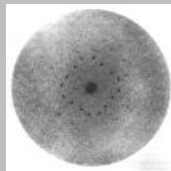
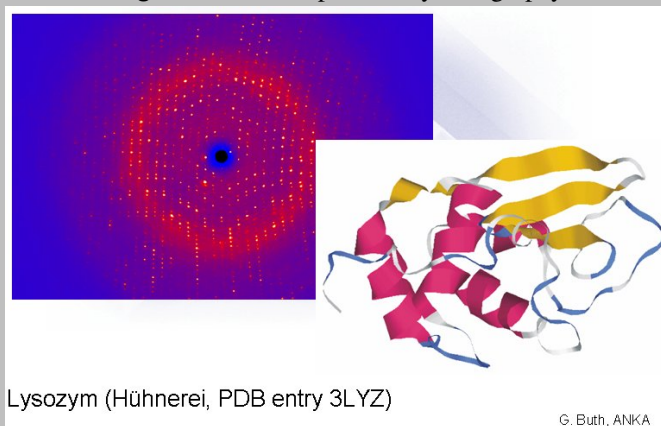


**Figure 6:** Max v. Laue: Laue diagram of zinc blende

**Figure 7:** Modern protein crystallography



Lysozym (Hühnerrei, PDB entry 3LYZ)

G. Buth, ANKA

Often it can be deduced from the structure of biological macromolecules (proteins, enzymes) to their functionality. Protein crystallography is one of the most important fields of application of synchrotron radiation. For this purpose, the macromolecules are crystallised, and the the structure factor of the unit cell, representing th molecular structure, is reconstruced from the intensity distribution of the reflections visible in the Laue diagram. For that purpose, of course, many reflections need to be recorded and evaluated with high signal to noise ratio, which in turn requires a high photon flux.



its application for synchrotron radiation sources. The interaction between method development on the user side and technological development on the accelerator side can, however, can only be kept in view to a certain extent. In this respect, for a more comprehensive picture, the courses that focus on the use of synchrotron radiation are recommended.

## References

- anonym, . (1900). *Photo of Wilhelm Conrad Röntgen*. URL: <https://commons.wikimedia.org/wiki/File:Roentgen2.jpg> (visited on 05/02/2019).
- Beck, P. et al. (Dec. 15, 2012). “The Redox State of Iron in the Matrix of CI, CM and Metamorphosed CM Chondrites by XANES Spectroscopy”. In: *Geochimica et Cosmochimica Acta* 99, pp. 305–316. ISSN: 0016-7037. DOI: [10.1016/j.gca.2012.04.041](https://doi.org/10.1016/j.gca.2012.04.041).
- Denecke, M. A. et al. (2005). “Spatially resolved micro X-ray fluorescence investigation of a uranium-rich sediment”. In: *Nachrichten - Forschungszentrum Karlsruhe* 37.4, pp. 175–178. ISSN: ISSN 0948-0919.
- Fenner, R. (June 26, 2013). *Lightning12*. URL: <https://www.flickr.com/photos/97432701@N03/9146367446/> (visited on 05/02/2019).
- Krewaldt, Robert (1894). *Heinrich Rudolf Hertz*. Published in *Lenard, P. (1930) Grosse Naturforscher, T.S. Lehmanns, Munich, 1930*. URL: [https://commons.wikimedia.org/wiki/File:Heinrich\\_Rudolf\\_Hertz.jpg](https://commons.wikimedia.org/wiki/File:Heinrich_Rudolf_Hertz.jpg) (visited on 05/02/2019).
- Matthias M. (Feb. 9, 2008). *Bragg*. URL: <https://commons.wikimedia.org/wiki/File:Bragg.svg> (visited on 05/09/2019).
- NASA - Fermi’s Best-Ever Look at the Gamma-Ray Sky (2020). URL: [https://www.nasa.gov/mission\\_pages/GLAST/news/gammaray\\_best.html](https://www.nasa.gov/mission_pages/GLAST/news/gammaray_best.html) (visited on 11/05/2020).
- Röntgen, Wilhelm (Jan. 23, 1896). *An Early X-ray Picture (Radiograph) Taken at a Public Lecture by Wilhelm Röntgen (1845–1923) of Albert von Kölliker’s Left Hand*. URL: [https://commons.wikimedia.org/wiki/File:X-ray\\_by\\_Wilhelm\\_R%C3%B6ntgen\\_of\\_Albert\\_von\\_K%C3%B6lliker%27s\\_hand\\_-\\_18960123-02.jpg](https://commons.wikimedia.org/wiki/File:X-ray_by_Wilhelm_R%C3%B6ntgen_of_Albert_von_K%C3%B6lliker%27s_hand_-_18960123-02.jpg) (visited on 05/09/2019).
- Sazanov, Sergei and Mike Revnivitsev (2006). *Ursprung kosmischer Röntgenstra*. URL: <https://www.mpg.de/361899/forschungsSchwerpunkt?c=166410> (visited on 05/03/2019).
- Schmutzer, Ferdinand (1921). *Albert Einstein during a Lecture in Vienna in 1921*. URL: [https://commons.wikimedia.org/wiki/File:Einstein\\_1921\\_by\\_F\\_Schmutzer\\_-\\_restoration.jpg](https://commons.wikimedia.org/wiki/File:Einstein_1921_by_F_Schmutzer_-_restoration.jpg) (visited on 05/02/2019).
- Sciences, The Royal Swedish Academy of (2012). *The Nobel Prize in Chemistry 2012*. Nobel-Prize.org. URL: <https://www.nobelprize.org/prizes/chemistry/2012/press-release/> (visited on 05/09/2019).
- Soleil Synchrotron, EPSIM 3D/JF Santarelli (Oct. 18, 2005). *Schema Des Françaischen Synchrotron Soleil*. URL: [https://commons.wikimedia.org/wiki/File:Sch%C3%A9ma\\_de\\_principe\\_du\\_synchrotron.jpg](https://commons.wikimedia.org/wiki/File:Sch%C3%A9ma_de_principe_du_synchrotron.jpg) (visited on 05/02/2019).
- Stodart, George J. (1890). *Engraving of James Clerk Maxwell by G. J. Stodart from a Photograph by Fergus of Greenock*. URL: [https://commons.wikimedia.org/wiki/File:James\\_Clerk\\_Maxwell.png](https://commons.wikimedia.org/wiki/File:James_Clerk_Maxwell.png) (visited on 05/02/2019).

Van de Kamp, Thomas et al. (Aug. 28, 2018). "Parasitoid Biology Preserved in Mineralized Fossils". In: *Nature Communications* 9.1, p. 3325. ISSN: 2041-1723. DOI: [10.1038/s41467-018-05654-y](https://doi.org/10.1038/s41467-018-05654-y).

## 2 Electrodynamics of moving point charges

The properties of synchrotron radiation, as exotic as they may seem, are of a fundamental nature. The physics of the electromagnetic fields radiated by accelerated charges from accelerated charges is, as H. Hertz has shown, completely contained in Maxwell's equations. For the physics of synchrotron radiation, the postulates of special relativity are added.

That it took a H. Hertz to deduce the properties of electromagnetic waves from Maxwell's equations, suggests, however, that Maxwell's equations do not reveal these properties too obviously. In this respect we will also spend some time on this.

### 2.1 Preface to the System of units

In electrostatics there are several different systems of units in use, in particular the *Gauß* or *cgs*- and the *SI* or *MKSA*- *MKSA*-system.

In addition, one finds the electrostatic (esu), the magnetostatic (emu) and the Heaviside-Lorentz system of units.

In this lecture, the *SI* system is used.

The SI system of units of electrostatics is given by the following relations of the vacuum natural constants (permeability, dielectric constant, velocity of light):

$$\mu_0 = 4\pi 10^{-7} \frac{\text{Vs}}{\text{Am}}, \quad \epsilon_0 \mu_0 c^2 = 1 \quad (2.1)$$

For the observables of classical electrostatics the following relations result for the translation between Gauß and SI system:

#### Electrodynamic systems of units

	Gauß	MKSA
Speed of light	$c$	$\sqrt{\mu_0 \epsilon_0}$
Electric field, potential	$\vec{E}, \Phi$	$\sqrt{4\pi \epsilon_0} \vec{E}, \Phi$
El. displacement field	$\vec{D}$	$\sqrt{\frac{4\pi}{\epsilon_0}} \vec{D}$
Charge density, charge, current density, current, polarisation	$\rho, q, \vec{j}, I, \vec{P}$	$\frac{1}{\sqrt{4\pi \epsilon_0}} \rho, q, \vec{j}, I, \vec{P}$
Magnetic flux density	$\vec{B}$	$\sqrt{\frac{4\pi}{\mu_0}} \vec{B}$
Magnetic field strength	$\vec{H}$	$\sqrt{4\pi \mu_0} \vec{H}$

The Gaußsystem is relatively widely used in the accelerator physics literature (which is not always explicitly mentioned). With the help of the table above, the formulas expressed in different systems of units can be translated into each other.

## 2.2 Integration of the inhomogeneous Maxwell equations

We start from the inhomogeneous Maxwell equations

$$\left. \begin{aligned} \operatorname{div} \vec{E} &= \frac{1}{\epsilon_0} \rho \\ \operatorname{rot} \vec{B} - \frac{1}{c^2} \frac{\partial \vec{E}}{\partial t} &= \mu_0 \vec{j} \end{aligned} \right\} \partial_\alpha F^{\alpha\beta} = \mu_0 J^\beta \quad (2.2)$$

$\vec{E}$  and  $\vec{B}$  can be derived from the electric and magnetic potentials

$$\left. \begin{aligned} \vec{B} &= \operatorname{rot} \vec{A} \\ \vec{E} + \frac{\partial \vec{A}}{\partial t} &= -\operatorname{grad} \phi \end{aligned} \right\} F^{\alpha\beta} = \partial^\alpha A^\beta - \partial^\beta A^\alpha \quad (2.3)$$

Under the Lorentz gauge condition

$$\operatorname{div} \vec{A} + \mu_0 \epsilon_0 \frac{\partial \phi}{\partial t} = 0 \quad \text{bzw.} \quad \partial_\alpha A^\alpha = 0 \quad (2.4)$$

substituting the potentials into the inhomogeneous Maxwell equations yields for each potential the inhomogeneous wave equation

$$\left. \begin{aligned} \Delta \phi - \frac{1}{c^2} \frac{\partial^2 \phi}{\partial t^2} &= -\frac{1}{\epsilon_0} \rho \\ \Delta \vec{A} - \frac{1}{c^2} \frac{\partial^2 \vec{A}}{\partial t^2} &= -\mu_0 \vec{j} \end{aligned} \right\} \square A^\beta = \mu_0 J^\beta(x) \quad (2.5)$$

The integration of the inhomogeneous wave gl. for each potential component (here in 4-potential notation) ?? is done by means of a Green function

$$A^\alpha(x) = A_{\text{hom}}^\alpha(x) + \mu_0 \int d^4x' G(x, x') J^\alpha(x') \quad (2.6)$$

with

$$\square G(x, x') = \delta(x^0 - x'^0) \delta(\vec{x} - \vec{x}') \quad (2.7)$$

Note:  $x, x'$  denote 4-vectors here,  $A_{\text{hom}}^\alpha(x)$  is the solution of the homogeneous wave equation.

*Remark.* In the absence of boundary conditions

$$G(x, x') = G(x - x'). \quad (2.8)$$

Solution of the equation 2.1 leads to two solutions (for the sake of clarity now explicitly written as a function of Cartesian space coordinates and time),

$$G_r(c(t-t'), \vec{x} - \vec{x}') = \begin{cases} 0 & \text{for } t-t' < 0 \\ \frac{1}{4\pi R} \delta(c(t-t') - R) & \text{for } t-t' > 0 \end{cases}$$

**retarded Green function**

$$G_a(c(t-t'), \vec{x} - \vec{x}') = \begin{cases} \frac{1}{4\pi R} \delta(c(t-t') - R) & \text{for } t-t' < 0 \\ 0 & \text{for } t-t' > 0 \end{cases}$$

**advanced Green function**

(2.9)

Thereby the spatial distance was introduced

$$R := |\vec{x} - \vec{x}'| \quad (2.10)$$

*Proof.* (sketch) The Green function can be calculated by a Fourier transformation of the inhomogeneous wave equation:

$$\left( \Delta - \frac{1}{c^2} \frac{\partial^2}{\partial t^2} \right) G(\vec{r}, t) = \delta(t-t') \delta(\vec{r} - \vec{r}')$$

$$\xrightarrow{FT} \left( \vec{k} \cdot \vec{k} - \frac{\omega^2}{c^2} \right) \hat{G}(\vec{k}, \omega) = \frac{1}{(2\pi)^2}$$
(2.11)

From this one obtains the Green function in space-time coordinates by back-transformation

$$G(\vec{r}, t) = \frac{c^2}{(2\pi)^4} \int d^3k \int d\omega \frac{e^{-i(\vec{k} \cdot \vec{r} - \omega t)}}{(\omega + ck)(\omega - ck)}$$

$$= \frac{c}{(2\pi)^2} \frac{1}{r} \frac{I(t)}{2i} (\delta(r-ct) - \delta(r+ct))$$
(2.12)

with the integral over the time component

$$I(t) := \int_{-\infty}^{\infty} du \frac{e^{-iut}}{u}$$
(2.13)

The evaluation of this integral with the help of the residue theorem leads to two solutions and thus to our two Green functions:

$$I^+(t) = \lim_{\epsilon \rightarrow 0^+} \int_{-\infty+i\epsilon}^{\infty+i\epsilon} du \frac{e^{-iut}}{u} = \begin{cases} 0 & \text{for } t < 0 \\ -2\pi i & \text{for } t > 0 \end{cases}$$

$$I^-(t) = \lim_{\epsilon \rightarrow 0^+} \int_{-\infty-i\epsilon}^{\infty-i\epsilon} du \frac{e^{-iut}}{u} = \begin{cases} 2\pi i & \text{for } t < 0 \\ 0 & \text{for } t > 0 \end{cases}$$
(2.14)

□

*Remark.* The retarded Green function is different from zero only on the forward light cone, the advanced one only on the backward light cone emanating from the source point  $x'$ . Solving the inhomogeneous wave equation 2.1 with the retarded (advanced) Green function, the solution of the homogeneous wave equation  $A_{\text{hom}}^\alpha(x)$  acquires the sense of an outgoing (incoming) wave for  $x_0 \rightarrow \infty$  ( $x_0 \rightarrow -\infty$ ).

The Green functions can be put into covariant (i.e. invariant under Lorentz transformations) form:

$$\begin{aligned} G_r(x-x') &= \frac{1}{2\pi} \theta(x^0 - x^{0'}) \delta\left((x-x')^2\right) \\ G_a(x-x') &= \frac{1}{2\pi} \theta(x^{0'} - x^0) \delta\left((x-x')^2\right) \end{aligned} \quad (2.15)$$

*Proof.*

$$\begin{aligned} \delta\left((x-x')^2\right) &= \delta\left((x^0 - x^{0'})^2 - |\vec{x} - \vec{x}'|^2\right) \\ &= \delta\left((x^0 - x^{0'} - R)(x^0 - x^{0'} + R)\right) \\ &= \frac{1}{2R} \left(\delta(x^0 - x^{0'} - R) + \delta(x^0 - x^{0'} + R)\right) \end{aligned}$$

□

The above applies in general to the integration of the inhomogeneous wave equation. In the following, this is now specialised to moving point charges.

### 2.3 Solution of the inhomogeneous wave equation for a point charge

Charge and current density of a point charge moving with respect to an inertial frame  $K$ :

$$\begin{aligned} \rho(\vec{x}, t) &= e \delta(\vec{x} - \vec{r}(t)) \\ \vec{j}(\vec{x}, t) &= e \frac{d\vec{r}}{dt} \delta(\vec{x} - \vec{r}(t)). \end{aligned} \quad (2.16)$$

Here (and in the following)  $r = (r^0, \vec{r})$  denotes a space-time point on the orbit of the point charge,  $x = (x^0, \vec{x})$  a general space-time point, henceforth the observation point.

This source term can be transformed with the 4-vector  $r^\alpha(\tau)$  as a function of the proper time  $\tau$  and the 4-velocity  $V^\alpha$  into the covariant form

$$J^\alpha(x) = e \int d\tau V^\alpha(\tau) \delta^{(4)}(x - r(\tau)) \quad (2.17)$$

*Remark.* Once again, as a reminder, in the inertial frame  $K$  the following applies:

$$\begin{aligned} r^\alpha &= (ct, \vec{r}(t)), \\ V^\alpha &= (\gamma c, \gamma \vec{v}) \end{aligned}$$

The integration of the inhomogeneous wave equation by means of a retarded Green function yields the *Liénard-Wiechert* potentials

$$A^\alpha(x) = \frac{\mu_0}{4\pi} \frac{eV^\alpha(\tau)}{V \cdot (x - r(\tau))} \Big|_{\tau=\tau_0} . \quad (2.18)$$

or in the more familiar non-covariant notation

$$\boxed{\begin{aligned} \phi(\vec{x}, t) &= \frac{1}{4\pi\epsilon_0} \left[ \frac{e}{(1 - \vec{\beta}(t') \cdot \vec{n}(t'))R(t')} \right]_{\text{ret}} \\ A(\vec{x}, t) &= \frac{\mu_0}{4\pi} \left[ \frac{e\vec{\beta}(t')}{(1 - \vec{\beta}(t') \cdot \vec{n}(t'))R(t')} \right]_{\text{ret}} \end{aligned}} \quad (2.19)$$

with the vector of the observation direction

$$\vec{n}(t') = \frac{\vec{x} - \vec{r}(t')}{R(t')} \quad (2.20)$$

and the *retardation condition*

$$\begin{aligned} (x - r(\tau_0))^2 &= 0 \\ \Leftrightarrow (t - t'(\tau_0)) - |\vec{x} - \vec{r}(\tau_0)|/c &= 0 \\ \Leftrightarrow t'(\tau_0) &= t - \frac{R(\tau_0)}{c} \end{aligned} \quad (2.21)$$

*Proof.* Execution of the spatial integral over the 4-current density with the Green function leads to

$$A^\alpha(x) = \frac{\mu_0}{2\pi} e \int d\tau V^\alpha \vartheta \left( x^0 - r^0(\tau) \right) \delta \left( (x - r(\tau))^2 \right) . \quad (2.22)$$

The residual integral over the proper time yields contributions only for  $\tau = \tau_0$ , where  $\tau_0$  is defined by the retardation condition

$$\begin{aligned} (x - r(\tau_0))^2 &= 0 \\ \Rightarrow (x^0 - r^0(\tau_0)) - |\vec{x} - \vec{r}(\tau_0)| &= 0 \end{aligned} \quad (2.23)$$

As is well known,

$$\delta [f(x)] = \sum_i \frac{\delta(x - x_i)}{\left| \left( \frac{df}{dx} \right)_{x=x_i} \right|} ,$$

if all  $x_i$  are simple zeros of  $f(x)$ . Furthermore,

$$\frac{d}{d\tau} (x - r(\tau))^2 = -2 (x - r(\tau))_\beta V^\beta(\tau) , \quad (2.24)$$

with zero  $\tau = \tau_0$ . Substitution and evaluation of the delta distribution in ?? leads to ??.  $\square$

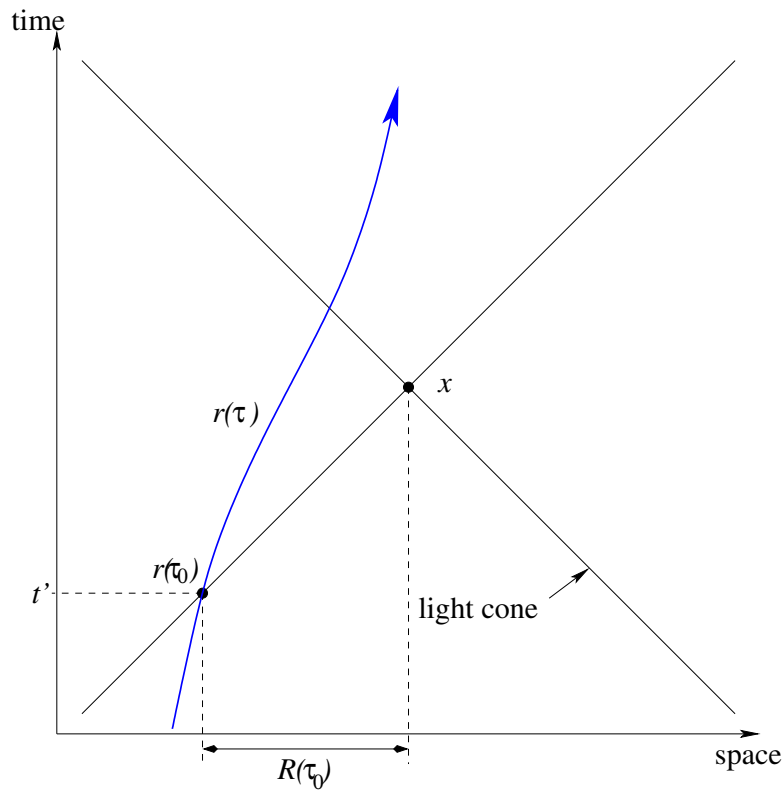


**Figure 9:** The retardation condition  $t'(\tau_0) = t - \frac{R(\tau_0)}{c}$

The retardation condition states that at the observation point  $x$  only an effect of the point charge can be observed that was caused by it at an intersection of its world line with the backward light cone. In other words, the effect (fields) of the moving charge propagates with (the finite) speed of light.

## 2.4 Derivation of the fields from the retarded potentials

The electromagnetic field tensor is derived from the 4-potential according to

$$F^{\alpha\beta}(x) = \partial^\alpha A^\beta - \partial^\beta A^\alpha. \quad (2.25)$$

Carrying out this differentiation yields

$$F^{\alpha\beta}(x) = \frac{e\mu_0}{4\pi} \frac{1}{V \cdot (x-r)} \frac{d}{d\tau} \left( \frac{(x-r)^\alpha V^\beta - (x-r)^\beta V^\alpha}{V \cdot (x-r)} \right) \Bigg|_{\tau=\tau_0}, \quad (2.26)$$

and finally in explicit, non-invariant form:

$$\vec{E}(\vec{x}, t) = \frac{e}{4\pi\epsilon_0} \left[ \frac{\vec{n} - \vec{\beta}}{\gamma^2(1 - \vec{\beta} \cdot \vec{n})^3 R^2} + \frac{1}{c} \frac{\vec{n} \times [(\vec{n} - \vec{\beta}) \times \dot{\vec{\beta}}]}{(1 - \vec{\beta} \cdot \vec{n})^3 R} \right]_{\text{ret}} \quad (2.27)$$

$$\vec{B}(\vec{x}, t) = \frac{1}{c} \left[ \vec{n} \times \vec{E} \right]_{\text{ret}}$$

with  $\vec{n}$  again being the directional vector from the emission point to the observation point in the laboratory system, and  $R$  the spatial distance between the emission and observation points in the laboratory system.

### Discussion

Equation ?? consists of two terms:

- |    |  |  |
|----|--|--|
| 1. | $\propto \vec{\beta}, \propto 1/R^2$     | velocity field<br>near field                       |
| 2. | $\propto \dot{\vec{\beta}}, \propto 1/R$ | acceleration field<br>far field<br>radiation field |

*Remark.* The static limit ( $\vec{\beta} = 0, \dot{\vec{\beta}} = 0$ ) of Eq. ?? is the Coulomb equation

$$\vec{E} = \frac{e\vec{n}}{4\pi\epsilon_0 R^2}. \quad (2.28)$$

*Remark.* The power flux density, given by the Poynting vector

$$\begin{aligned} \vec{S} &= \frac{1}{\mu_0} (\vec{E} \times \vec{B}) \Big|_{\text{ret}} \\ &= \frac{1}{\mu_0 c} \vec{E} \times (\vec{n} \times \vec{E}) \Big|_{\text{ret}} \\ &= \frac{1}{\mu_0 c} (E^2 \vec{n} - (\vec{n} \cdot \vec{E}) \vec{E}) \Big|_{\text{ret}}, \end{aligned} \quad (2.29)$$

is proportional to  $E^2$  has three contributions:

- |    |                              |                 |
|----|------------------------------|-----------------|
| 1. | near field contribution      | $\propto 1/R^4$ |
| 2. | radiation field contribution | $\propto 1/R^2$ |
| 3. | mixed term                   | $\propto 1/R^3$ |

The total emitted power can be calculated by integrating the Poynting vector over a sphere. Doing so, it turns out that only the radiation field term contribution is independent of  $R$ , whereas the other two become negligible for large  $R$ .

In other words: Only the radiation field contribution transports power into open space.

Therefore in the following the drop the near field terms, which is called the far field approximation.

## 2.5 radiated field and emitted power

In the following, we will now discuss the radiation term of the electric field in order to determine the emitted radiation power and its angular distribution. For this purpose, the following preliminary remark on *emitted* and *observed* radiation fields.

*Remark.* The time dependence of the radiation field observed at time  $t$ , which was emitted at a time  $t' = t - R(t)/c$ , obviously depends on the relation between emission and observation time. In particular, an energy emitted during an emission time interval  $\Delta t'$  can arrive at the observer during a much shorter time interval  $\Delta t$ .

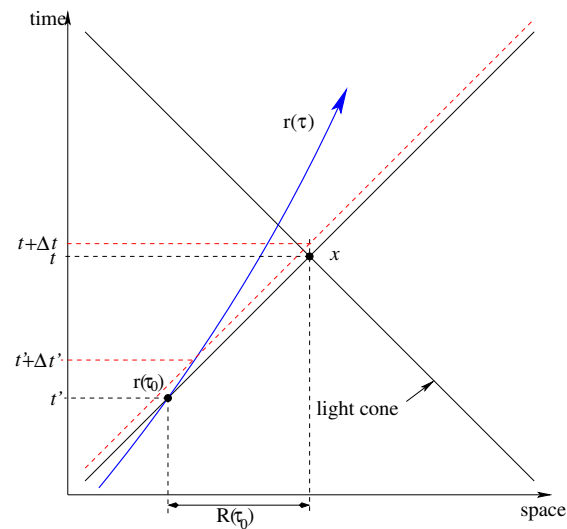


**Figure 10:** relationship between emission and observation time interval

This leads to the necessity of distinguishing emitted power  $P(t')$  and observed power  $P_x(t)$ . The full information about the angular and spectral distribution of the radiation to be observed is of course contained in the expressions for the observed power. On the other hand, the emitted and observed energy and thus also the time-averaged emitted and observed power must be the same. Therefore, it is possible to derive some essential properties of synchrotron radiation from the expression for the emitted power  $P(t')$ . As we shall see in a moment, this is a considerable simplification, since the consideration becomes independent of the explicit relation between observation and emission time. What is lost, however, is the information about the spectral properties of the radiation. We will gain this information later from the discussion of the special cases relevant to us.

Transition from the observed (retarded) to the emitted radiation field:

The Poynting vector of the radiation field is:

$$\vec{S} = \frac{E^2}{\mu_0 c} \vec{n} \quad (2.30)$$

$$= \frac{1}{R^2} \frac{d^2 W}{d\Omega dt} \vec{n}. \quad (2.31)$$

That is, the Poynting vector represents the energy flux per observer time interval per unit area  $R^2 d\Omega$ .

Let us now consider the *emitted power flux*

$$\begin{aligned} \frac{dP}{d\Omega} &:= \frac{d^2W}{d\Omega dt'} \\ &= \frac{d^2W}{d\Omega dt} \frac{dt}{dt'} \end{aligned} \quad (2.32)$$

Thus, to consider the emitted power, only the relation of the *time differentials* is relevant,

$$\begin{aligned} dt &= \frac{dt}{dt'} dt' \\ &= \frac{d}{dt'} \left( t' + \frac{R(t')}{c} \right) dt' \\ &= (1 - \vec{n} \cdot \vec{\beta}) dt', \end{aligned} \quad (2.33)$$

not the dependency  $t(t')$ .

We thus obtain

$$\boxed{\frac{dP}{d\Omega} = \frac{R^2 |\vec{E}|^2}{\mu_0 c} (1 - \vec{n} \cdot \vec{\beta})} \quad (2.34)$$

Every instantaneous acceleration can be divided into a longitudinal and a transversal component. Technically, one of these components usually occurs in each case: In the case of deflection by magnetic fields, there is no longitudinal component; electric fields (in particle accelerators) are usually used for longitudinal acceleration alone. As we will see, practically only the transverse case plays a role in the generation of synchrotron radiation.

## 2.6 Transverse and longitudinal acceleration

### The coordinate system

In the following, the following coordinate system is used: The positively (!) charged particle moves in positive  $z$ -direction through the origin at the time of emission and is accelerated either transversely by a homogeneous magnetic field directed in negative  $y$ -direction or longitudinally by an electric field directed in positive  $z$ -direction (the figure shows the transverse case treated first).

The general observation point is called  $P$ , the corresponding position vector (= distance vector from the charge to the observation point)  $\vec{R}$ . Also drawn are the polar coordinates  $(\vartheta, \varphi)$ .

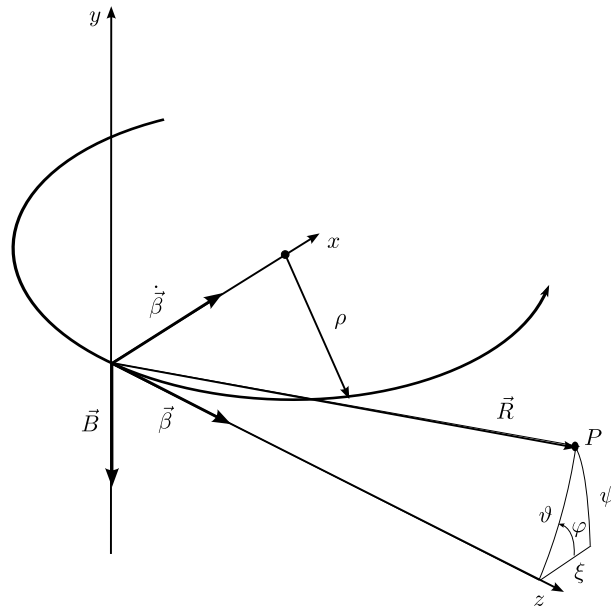


**Figure 11:** Coordinate system for the description of normal synchrotron radiation

In these coordinates

$$\vec{n} = \begin{pmatrix} \sin \vartheta \cos \varphi \\ \sin \vartheta \sin \varphi \\ \cos \vartheta \end{pmatrix} \quad \text{unit vector in direction of observation} \quad \vec{\beta} = \beta \begin{pmatrix} 0 \\ 0 \\ 1 \end{pmatrix} \quad (2.35)$$

### Transverse acceleration

Let a positively charged particle of normalised velocity  $\beta$  move in a magnetic field  $\vec{B}$  pointing in the  $-y$  direction. Then it is momentarily moving on a circular path whose radius is given by equating the centripetal and Lorentz forces:

$$\begin{aligned} \frac{\gamma m (c\beta)^2}{\rho} &= ec\beta B \\ \Leftrightarrow \frac{1}{\rho} &= \frac{eB}{mc\beta\gamma} \end{aligned} \quad (2.36)$$

Thus

$$\vec{\beta} = \begin{pmatrix} 0 \\ 0 \\ 1 \end{pmatrix}, \quad \dot{\vec{\beta}} = \frac{\beta^2 c}{\rho} \begin{pmatrix} 1 \\ 0 \\ 0 \end{pmatrix} \quad (2.37)$$

This is inserted into the expression for the radiation term in Eq. ?? yields

$$\vec{E} = -\frac{e\beta^2}{4\pi\epsilon_0 R\rho} \frac{1}{(1 - \beta \cos \vartheta)^3} \begin{pmatrix} 1 - \beta \cos \vartheta - \sin^2 \vartheta \cos^2 \varphi \\ -\sin^2 \vartheta \cos \varphi \sin \varphi \\ -\sin \vartheta \cos \varphi (\cos \vartheta - \beta) \end{pmatrix} \quad (2.38)$$

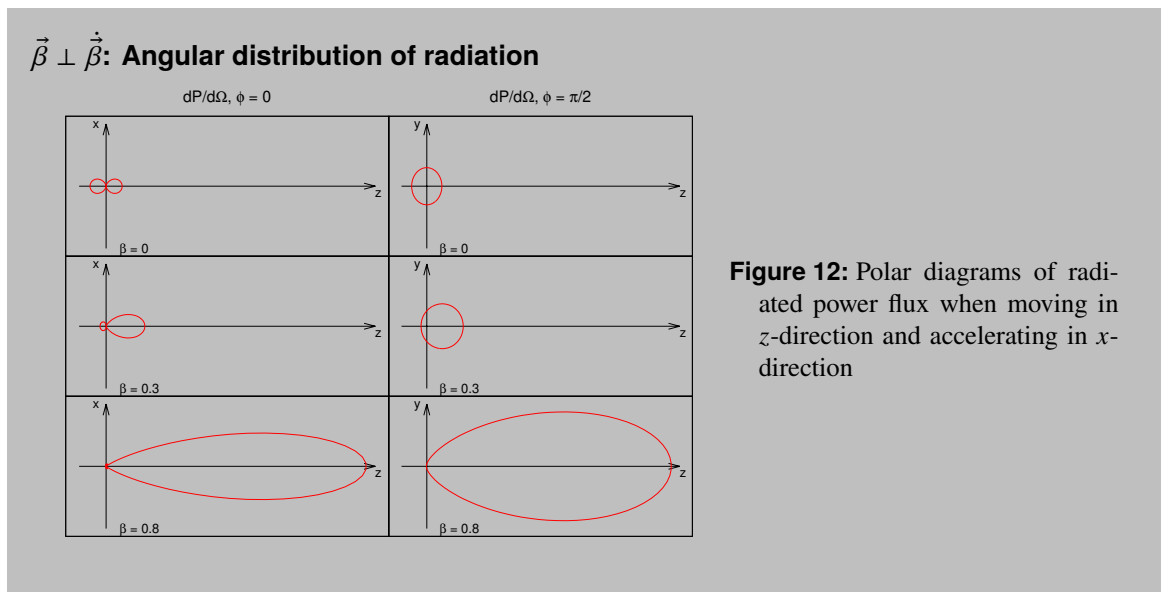
and with Eq. ?? finally for the power flow:

Power flow:

$$\frac{dP_{\perp}}{d\Omega} = \frac{3}{2} \frac{P_{\perp 0}}{4\pi\gamma^4} \frac{(1 - \beta \cos \vartheta)^2 - (1 - \beta^2) \sin^2 \vartheta \cos^2 \varphi}{(1 - \beta \cos \vartheta)^5} \quad (2.39)$$

With the radiant power integrated over the solid angle

$$P_{\perp 0} = \frac{2}{3} \frac{e^2 \dot{\beta}^2 \gamma^4}{4\pi\epsilon_0 c} \quad (2.40)$$



### Transverse acceleration, ultrarelativistic case

*Remark.* The angular distribution of the radiant power flux has a nodal line at

$$\vartheta_0 = \arccos \beta,$$

which in the ultra-relativistic case tends to

$$\lim_{\gamma \rightarrow \infty} \vartheta_0 = \frac{1}{\gamma}.$$

Overall, the fraction of radiated power into a cone with opening angle  $\vartheta_0$ :

$$\frac{1}{P_{T0}} \int_{\vartheta \leq \vartheta_0} d\Omega \frac{dP}{d\Omega} = \frac{1}{2} \left( 1 + \frac{9}{16} \beta \right) \geq \frac{1}{2} \quad \forall \beta$$

Thus, in the ultrarelativistic case, the emission angles are of order  $\frac{1}{\gamma}$  and it can be approximated

$$\begin{aligned} 1 - \beta \cos \vartheta &\approx 1 - \beta + \frac{\beta \vartheta^2}{2} \\ &= \frac{1 - \beta^2}{1 + \beta} + \frac{\beta \vartheta^2}{2} \\ &\approx \frac{1}{2\gamma^2} (1 + \gamma^2 \vartheta^2) \end{aligned} \quad (2.41)$$

Thus

$$\vec{E} = -\frac{e\gamma^4}{\pi\epsilon_0 R\rho} \frac{1}{(1 + \gamma^2 \vartheta^2)^3} \begin{pmatrix} (1 - \gamma^2 \vartheta^2) \cos \varphi \\ -(1 + \gamma^2 \vartheta^2) \sin \varphi \\ 0 \end{pmatrix} \quad (2.42)$$

*Remark.* From this we can already read the essentials of polarisation.

With these approximations the angular distribution of the radiated power can be written:

$$\begin{aligned} \frac{dP_{\perp}}{d\Omega} &= P_{\perp 0} \frac{3\gamma^2}{\pi} \frac{1 - 2\gamma^2 \vartheta^2 \cos(2\varphi) + \gamma^4 \vartheta^4}{(1 + \gamma^2 \vartheta^2)^5} \\ P_{\perp 0} &= \frac{2}{3} \frac{r_0 c m c^2 \gamma^4}{\rho^2} \end{aligned} \quad (2.43)$$

Here we introduced the classical particle radius

$$r_0 := \frac{e^2}{4\pi\epsilon_0 m c^2}. \quad (2.44)$$

Here, as above, it is assumed that the charged particle is kept on its circular path by a constant magnetic field. Note: For a given circular path (as is the case in the synchrotron), the radiated power goes with  $\gamma^4$ . The radiation angle  $\vartheta$  scales with  $\gamma$ .

$\vec{\beta} \perp \dot{\vec{\beta}}$ : ultra-relativistic case

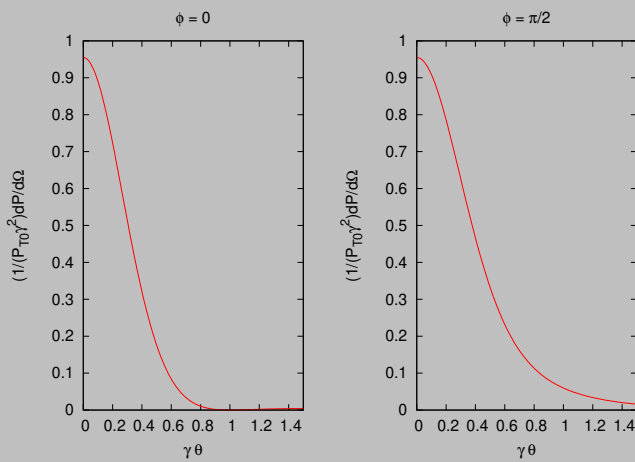
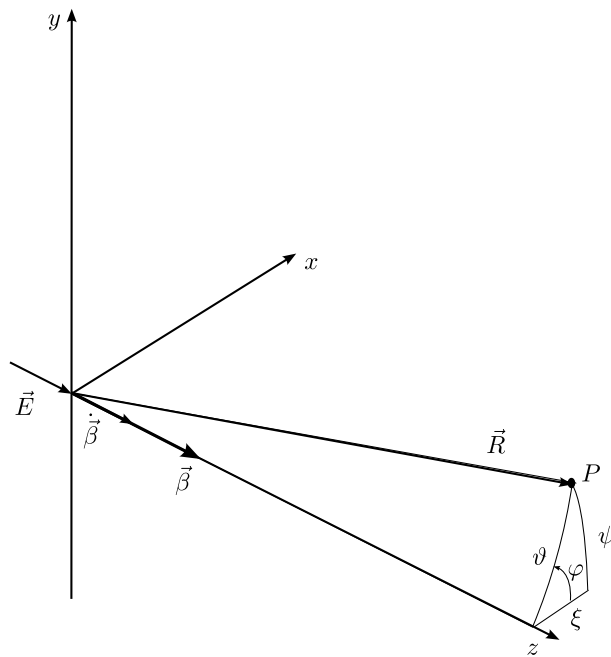


**Figure 13:** angular distribution of radiant power under transverse acceleration in the ultrarelativistic case

**Longitudinal acceleration**



In this case

$$\vec{\beta} = \begin{pmatrix} 0 \\ 0 \\ 1 \end{pmatrix} \quad \dot{\vec{\beta}} = \dot{\beta} \begin{pmatrix} 0 \\ 0 \\ 1 \end{pmatrix} \tag{2.45}$$

and thus

$$\vec{\beta} \times \dot{\vec{\beta}} = 0. \quad (2.46)$$

In the same way as for the transversal case we get

$$\frac{dP_{\parallel}}{d\Omega} = \frac{e^2 \dot{\vec{\beta}}^2}{(4\pi)^2 \epsilon_0 c} \frac{\sin^2 \vartheta}{(1 - \beta \cos \vartheta)^5} \quad (2.47)$$

$$= \frac{3}{2} \frac{P_{\parallel 0}}{4\pi \gamma^6} \frac{\sin^2 \vartheta}{(1 - \beta \cos \vartheta)^5} \quad (2.48)$$

$$\text{with } P_{parallel0} = \frac{2}{3} \frac{r_0 m c^2 \dot{\vec{\beta}}^2 \gamma^6}{c} \quad (2.49)$$

again being the integral radiant power.

### $\vec{\beta} \parallel \dot{\vec{\beta}}$ : Angular distribution of radiation

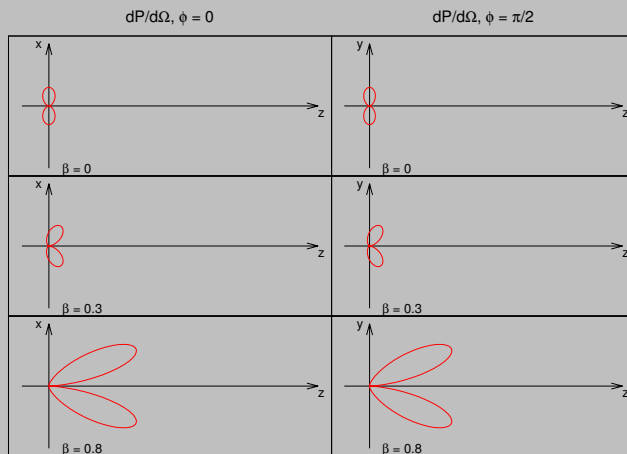


**Figure 14:** Polar diagrams of radiated power flux when moving in  $z$ -direction and accelerating in  $z$ -direction

$$\text{angle of maximum radiation: } \cos \vartheta_m = \frac{\sqrt{1 + 15\beta^2} - 1}{3\beta} \quad (2.50)$$

*Remark.* In the longitudinal case, the radiation fields are cylindrically symmetric about  $z$ .

### Longitudinal acceleration, ultrarelativistic case

For the longitudinal case and the angle of maximum radiation, the same approximations can be derived as for the transverse acceleration:

$$\frac{dP_{\parallel}}{d\Omega} = P_{\parallel 0} \frac{12\gamma^2}{\pi} \frac{\gamma^2 \vartheta^2}{(1 + \gamma^2 \vartheta^2)^5}, \quad \lim_{\beta \rightarrow 1} \vartheta_m = \frac{1}{2\gamma} \quad (2.51)$$

**Discussion: momentum change and radiated power**

In order to correctly interpret the results found for the radiated power under longitudinal transversal acceleration, these must be related to the *momentum* change, i.e. to the Lorentz force acting in each case. For this purpose, let us once again consider the equation of motion:

$$\frac{d \text{iff} \vec{p}}{dt} = m\gamma \frac{d \text{iff} \vec{v}}{dt} + m\vec{v} \frac{d}{dt} \quad (2.52)$$

But it is

$$\begin{aligned} \frac{d\gamma}{dt} &= \frac{d\gamma}{d\beta} \frac{d\beta}{dt} \\ &= \gamma^3 \frac{\beta}{c} \frac{dv}{dt}. \end{aligned}$$

Therefore

$$\frac{d\vec{p}}{dt} = m\gamma \frac{d\vec{v}}{dt} + m\gamma^3 \frac{\beta}{c} \frac{dv}{dt} \vec{v}. \quad (2.53)$$

From this we can derive for the transversal and the longitudinal equation of motion:

**case 1:**  $\vec{F} \parallel \vec{v} \longrightarrow \dot{v}\vec{v} = \dot{v}v$

It follows:

$$\boxed{\frac{d\vec{p}_{\parallel}}{dt} = m\gamma \left(1 + \gamma^2 \beta \frac{v}{c}\right) \frac{d\vec{v}_{\parallel}}{dt} = m\gamma^3 \frac{d\vec{v}_{\parallel}}{dt}.} \quad (2.54)$$

**case 2:**  $\vec{F} \perp \vec{v} \longrightarrow \frac{dv}{dt} = 0.$

It follows:

$$\boxed{\frac{d\vec{p}_{\perp}}{dt} = m\gamma \frac{d\vec{v}_{\perp}}{dt}} \quad (2.55)$$

Thus, in summary:

$$\dot{\vec{p}}_{\perp} = m\gamma c \dot{\vec{\beta}}_{\perp} \qquad \dot{\vec{p}}_{\parallel} = m\gamma^3 c \dot{\vec{\beta}}_{\parallel},$$

and thus

$$P_{\perp 0} = \frac{2}{3} \frac{r_0 \dot{\vec{p}}_{\perp}^2 \gamma^2}{mc} \qquad P_{\parallel 0} = \frac{2}{3} \frac{r_0 \dot{\vec{p}}_{\parallel}^2}{mc} \quad (2.56)$$